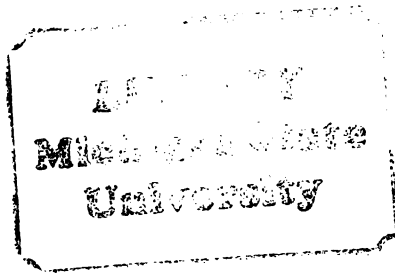




104
476
THS



This is to certify that the

thesis entitled

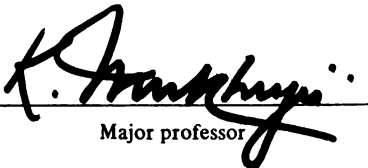
FAILURE CRITERION OF A MULTI-LAYERED
GLASS-FIBER-REINFORCED-EPOXY COMPOSITE
MATERIAL AND THE APPLICABILITY OF THE
STREE FIELD THEORY

presented by

Ching-Fong Chen

has been accepted towards fulfillment
of the requirements for

M.S. degree in Metallurgy


Major professor

Date Feb 7, 1983.



RETURNING MATERIALS:
Place in book drop to
remove this checkout from
your record. FINES will
be charged if book is
returned after the date
stamped below.

--	--	--

FAILURE CRITERION OF A MULTI-LAYERED GLASS-FIBER-
REINFORCED-EPOXY COMPOSITE MATERIALS
AND
THE APPLICABILITY OF THE STRESS FIELD THEORY

By

Ching-Fong Chen

A THESIS

submitted to
Michigan State University
in partial fulfillment of the requirements
for the degree of

MASTER OF SCIENCE

Department of Metallurgy, Mechanics and Materials Science

1983

ABSTRACT

FAILURE CRITERION OF A MULTI-LAYERED GLASS-FIBER- REINFORCED-EPOXY COMPOSITE MATERIAL AND THE APPLICABILITY OF THE STRESS FIELD THEORY

By

Ching-Fong Chen

6120580

Mechanical properties of a composite were experimentally investigated as a function of the orientation. These results can be explained by a superposition of failure criteria of the fiber failure mode and the matrix failure mode. The nature of the failure mode as a function of fiber orientation, θ , was examined by using optical and scanning electron microscopy. Some preliminary investigations were also conducted to determine the elastic stress-strain distributions. For that purpose, a laser interferometric strain gage (I.S.G.) measuring system was used. The adaptation of this technique to a poorly reflecting composite material poses some experimental difficulties. These difficulties were overcome by a successful bonding of a metallic layer on the surface of the sample. Preliminary results of the I.S.G. investigation indicate a free-edge effect of the stress-strain distribution in accordance with existing theories.

ACKNOWLEDGMENTS

This research is partially supported by the Ford Motor Company. I would like to thank Mr. Subhasish Sircar and Mr. Brian B. Schultz for their help in accomplishing some of the experimental work. Dr. Masaharu Kato is also appreciated for the data analysis. I would like to thank Dr. John F. Martin for his guidance throughout the work, especially for giving me the chance to use the I.S.G. equipment. Special thanks goes to Dr. Kalinath Mukherjee. He offered me the chance to do this topic and gave me inspiration and guidance constantly. Without his help this thesis could not have been finished. He is an excellent teacher, a friend and the advisor.



TABLE OF CONTENTS

LIST OF FIGURE	iv
I. INTRODUCTION	1
II. EXPERIMENTAL METHODS	6
(a) Material and Sample Preparation	6
(b) Tensile Test	6
(c) Scanning Electron Microscopy	6
(d) Computer Analysis and Calculation	13
(e) Fundamentals of the Interferometric Strain Gage (I.S.G.)	13
(f) Application of the I.S.G. Technique for an Epoxy Composite	20
(g) Cyclic Stress-Strain Test	25
III. RESULTS AND DISCUSSION	27
(a) Static Tensile Properties	27
(b) Failure Criterion	31
(c) Validity of I.S.G. Technique for Composites	41
(d) Stress Distribution Across the Top Surface	44
IV. CONCLUSIONS	46
APPENDIX: Tensor Transformation	47
LIST OF REFERENCES	49



LIST OF FIGURES

Figure	Page
1. Unidirectional Layer of the Composite	7
2. Multidirectional Layer of the Composite	8
3. Three Dimensional Schematic of the Laminate	9
4. Geometry of Tensile Sample	10
5. Geometry of Cyclic Loading Sample	11
6. Locations of the Indentations for the I.S.G. on a Test Sample	12
7. Interferometric Strain Gage	14
8. Fundamental of I.S.G.	15
9. Indentations on Sample (S E M Micrograph)	16
10. Interference Pattern	17
11. Schematic Diagram for the Laser Interferometric Strain Measuring System	19
12. The Indentation in the Region that Contains Both Fibers and Epoxy	22
13. Indentations in the Region that Contains Epoxy Only	23
14. Geometry of the Indentation	24
15. Schematic Stress-Strain Behavior of a Linear Elastic Material	28
16. Schematic Stress-Strain Behavior of a Viscoelastic Material	28
17. Tensile Stress-Strain Curve of the Composite for Different Orientations	29
18. Schematic Presentation of the Three Regions of the Tensile Stress-Strain Curve	30

Figure	Page
19. Comparison of Fracture Surface for Various Orientations	32
20. SEM Micrograph of a 0° Sample	33
21. SEM Micrograph of a 90° Sample	35
22. SEM Micrograph of a 90° Sample	36
23. Positive Rotation of Principal Material Axes from Arbitrary X-Y Axes	37
24. $n = 1.20$	40
25. $n = 1.16$	40
26. Static Strength vs. Angle	42
27. Extensometer Strain vs. Stress	43
28. Distribution of σ_x Along Surface of the Sample	45

I. INTRODUCTION

An operationally simple strength tensor theory for fiber reinforced composites has been proposed by Tsai and Wu(1). This theory has increased the ability of curve fitting based on the prediction

$$F_i \sigma_i + F_{ij} \sigma_i \sigma_j = 1 \quad (1)$$

where F_i and F_{ij} are strength tensors, and $i, j = 1, 2, \dots, 6$.

Hashin and Rotem (2) used a simple failure criterion to predict the deformation of an unidirectional fiber reinforced laminae. This approach is based on the two different failure modes. One is the fiber-failure mode and the other is the matrix-failure mode.

For the former mode,

$$\sigma_A = \sigma \cos^2 \theta \quad (2)$$

criterion was used,

where,

$\sigma_A = \sigma_{11}$ is the stress in the fiber direction.

σ is the applied stress.

θ is the angle between applied stress and the fiber direction.

For the latter mode,

$$\left(\frac{\sigma_T}{\sigma_T^S}\right)^2 + \left(\frac{\tau}{\tau^S}\right)^2 = 1 \quad (3)$$

criterion was used,

where,

$$\sigma_T = \sigma_{22}$$

$$\tau = \sigma_{12}$$

σ_T^S is the failure stress in transverse loading alone.

τ^S is the failure stress in shear loading alone.

The critical angle θ_c , up to which equation (2) holds, can also be calculated from this theory,

$$\tan \theta_c \approx \frac{\tau^S}{\sigma_A^S} \quad (4)$$

Rotem (3) extended the application of this theory to the angle plies laminae with various reinforcement angles under different strain fields. Rotem (4) also proposed a general fatigue failure criterion for multidirectional laminate. The static failure is expressed by:

$$\sigma_A^S = K_{xx} \sigma^S \quad (5)$$

$$\sigma^S = \left[\left(\frac{K_{yy}}{\sigma_T} \right)^2 + \left(\frac{K_{xy}}{\tau} \right)^2 \right]^{-\frac{1}{2}} \quad (6)$$

where,

σ^S is the failure stress.

$$K_{xx} = \frac{1}{2} \left[1 - \sec 2\theta + \frac{(\mu + \sec 2\theta) \tan^2 2\theta}{\eta + \tan^2 2\theta} \right]$$

$$K_{xy} = -\frac{1}{2} \frac{(\mu + \sec 2\theta) \tan 2\theta}{\eta + \tan^2 2\theta}$$

The composite material that is studied in this program is neither a unidirectional laminate nor a multidirectional laminate. This material consists of alternate unidirectional and random reinforced layers. Hence in the present case, a simplified approach is adopted. This approach is based upon the strength theory of Tsai and Wu, and failure criterion of Hashin and Rotem. In stead of assuming the quadratic form for the matrix failure mode, an exponent n shall be used for this special material, i.e.

$$\left(\frac{\sigma_2}{\sigma_2^S} \right)^n + \left(\frac{\tau_{12}}{\tau_{12}^S} \right)^n = 1 \quad (7)$$

where σ_2^s , σ_{12}^s are material constants. For the fiber-failure mode, the experimental result shows that the angle is very small and the strength does not change very much within this range. Hence, we shall assume that:

$$\sigma_f = \sigma_o \cos^2 \theta$$

where σ_o is the failure stress of the 0° sample.

Recently attention has been given to the problem of stress distributions in laminated plates. It is well known that laminated plate theory (LPT) takes into account the stresses in the plane of the laminate, σ_x , σ_y and τ_{xy} ; namely, a plane stress state is assumed. Puppo and Evensen (5) proposed a model in which a set of anisotropic layers are separated by isotropic adhesive layers. They assumed that each anisotropic layer carries only inplane loads and exists in a state of generalized plane stress, while the isotropic layers carry the interlaminar shear stress.

After these, Pipes and Pagano (6) obtained the solution for the exact equations of elasticity on the free edge region. For this solution a symmetric laminate under uniform axial stress was assumed. The Moiré technique was utilized by Pipes (7) to examine the surface displacement of the symmetric angle-ply laminate under axial extension. Pagano (8) proposed a new theory to define the complete stress field with an arbitrary composite laminate. The results were compared with

the numerical results by Wang and Crossman (9).

In order to develop a general characterization of the various failure modes, it is necessary to have a practical means of laminate stress analysis. The finite element method has been widely used by some authors (10, 11). This is accomplished through the assumption of a simplified displacement field according to the classical lamination theory. Hence, its application is limited to the determination of the force distribution rather than the stress distribution. Therefore, experimentation is the primary method so far to find the stress distribution in order to determine the failure loading and mode of fracture.

An Interferometric Strain Gage (I.S.G.) is a very powerful technique for measuring the local stress-strain behavior (12, 13, 14, 15). Unfortunately, its application is mostly limited to the metallic materials, because the necessary condition for using the I.S.G. is to have a very smooth reflecting surface. The composite materials are not very good reflecting materials. Thus, in order to apply this technique to composite materials, it is necessary to metallize the surface. There are several ways to metallize an epoxy composite surface, e.g., vapor deposition, coating, etc.. A relatively successful metallizing technique was developed for the present case. Using such a technique the surface stress distribution of our laminate is experimentally determined and these results are compared with the stress distributions predicted by Wang and Crossman (9), and Pagano (8).

II. EXPERIMENTAL METHODS

(a) Material and Sample Preparation:

In this material, a set of unidirectional layers (Figure 1) are separated by adhesive layers containing multidirectional random fibers (Figure 2) to form a sandwich structure. The three dimensional schematic structure (Figure 3) shows that all the unidirectional layers are reinforced in the same direction and all the multidirectional layers are in the random array. The angle θ is defined as the angle between the unidirectional reinforced direction and the applied load σ_x . By using this angle θ , the static tensile samples were made at the following angles: 0° , 15° , 30° , 45° , 60° , and 90° . In order to avoid those problems of slipping out and fracture at the grip, the geometry of the static tensile sample is designed as shown in Figure 4.

The geometry of the cyclic loading sample is shown in Figure 5. The cyclic loading sample was made in the 0° direction and the locations of the indentations are made along the top of the sample as shown in Figure 6.

(b) Tensile Test:

All tensile samples were tested by using an Instron Floor Model tensile testing machine.

(c) Scanning Electron Microscopy:

The fracture surface of the 0° and 90° samples were observed by





Figure 1 : Unidirectional Layer of the Composite

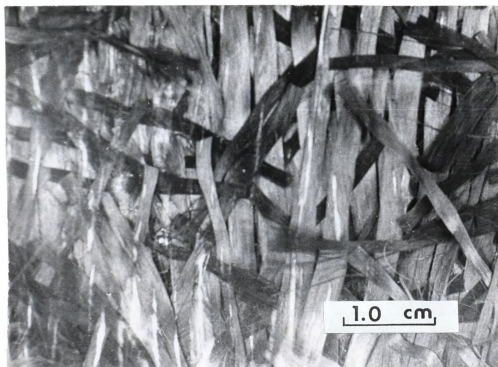
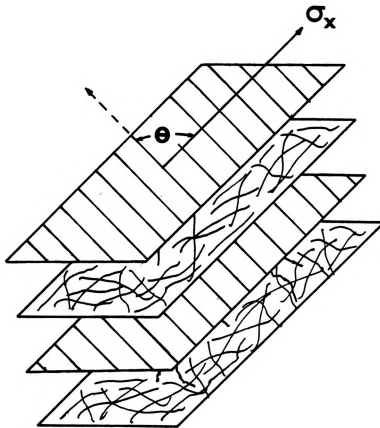


Figure 2 : Multidirection Layer of the Composite



**Figure 3 : Three Dimensional Schematic
of the Laminate**

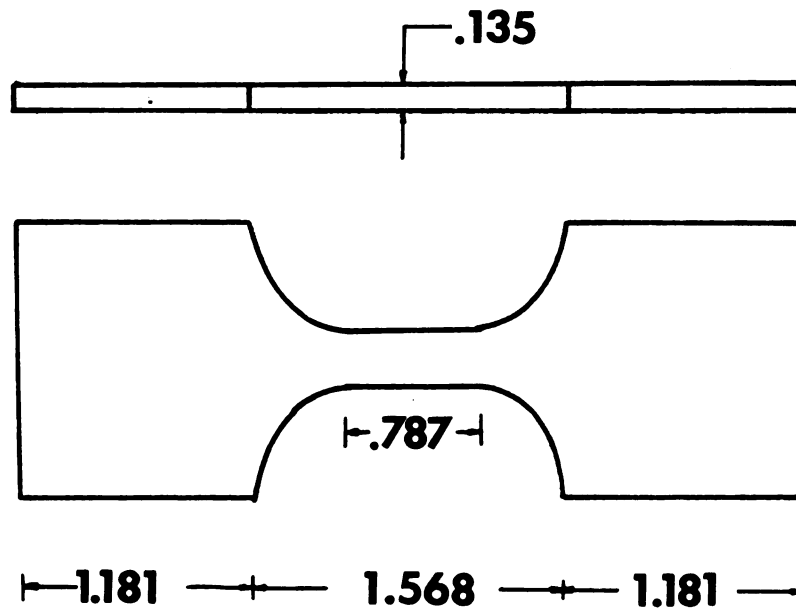


Figure 4 : Geometry of Tensile Sample
(Unit : inch)

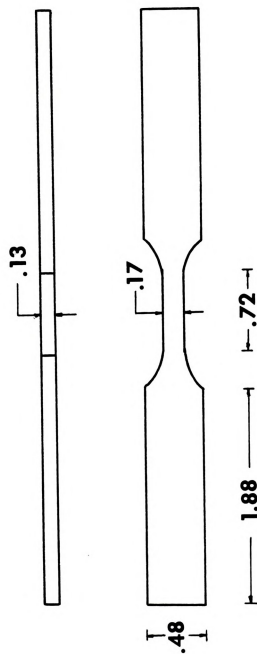
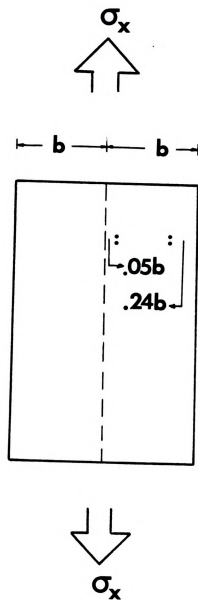
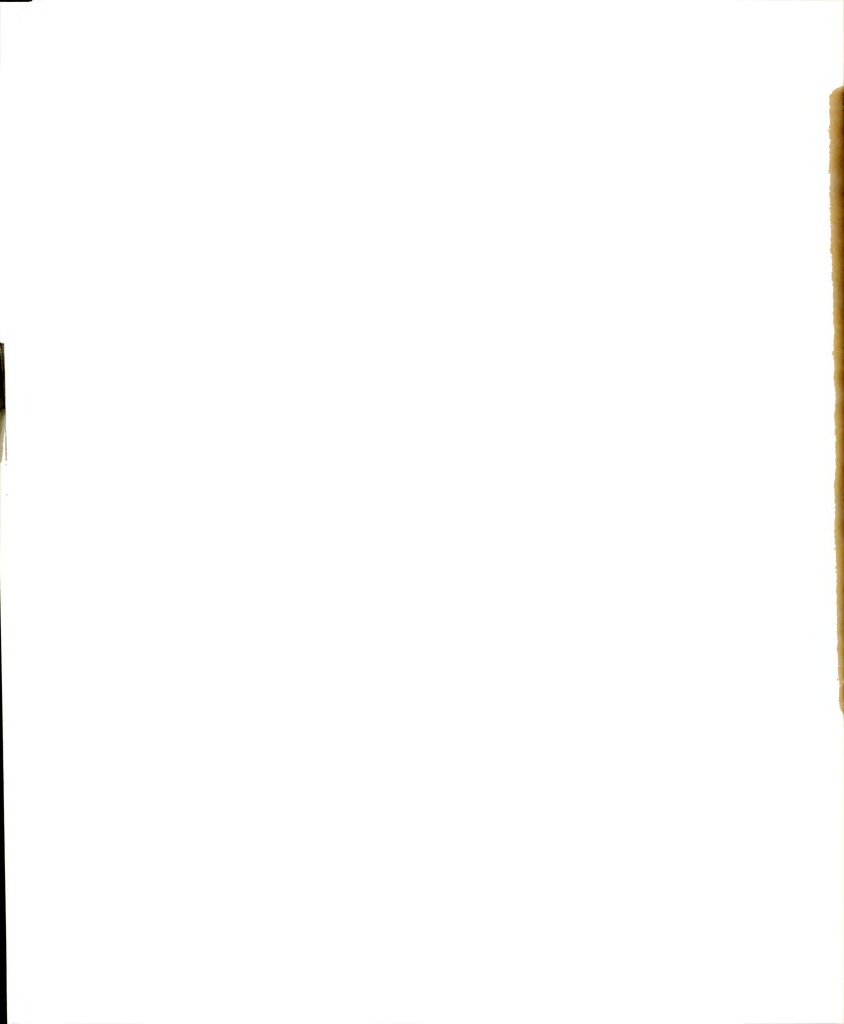


Figure 5 : Geometry of Cyclic Loading Sample
(Unit : inch)



**Figure 6 : Locations of the Indentations
for the I.S.G. on a Test
Sample**



using the scanning electron microscope (HITACHI Model 415A). For electron conduction in these nonmetallic materials, the samples were metalized by vacuum vapor deposition. The coating material used was copper.

(d) Computer Analysis and Calculation:

Newton interpolation polynomial method was used for curve fitting experimental data. The transition angle, θ_c , between the two different failure modes was also calculated by using the computer.

(e) Fundamentals of the Interferometric Strain Gage (I.S.G.):

The Interferometric Strain Gage (I.S.G.) is a noncontacting Laser based measuring system which can measure strains over a very small gage length (50-100 microns). Figure 7 shows the set-up of I.S.G.. Figure 8 illustrates the fundamental principles upon which the I.S.G. is designed. A Vicker's hardness tester, with a pyramidal diamond, was used to get the indentations which form a gage length on a sample Figure 9. Incident monochromatic coherent laser light is reflected by the indentations. These reflecting rays interfere to create interference fringes (Figure 10) when the following relation is satisfied:

$$d \sin \alpha = n \lambda \quad (n = 0, \pm 1, \pm 2, \dots) \quad (9)$$

where: λ = wavelength of the laser light

n = order of reflection

d = space between two indentations

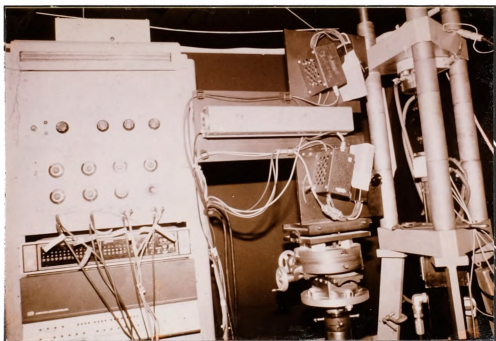


Figure 7: Interferometric Strain Gage

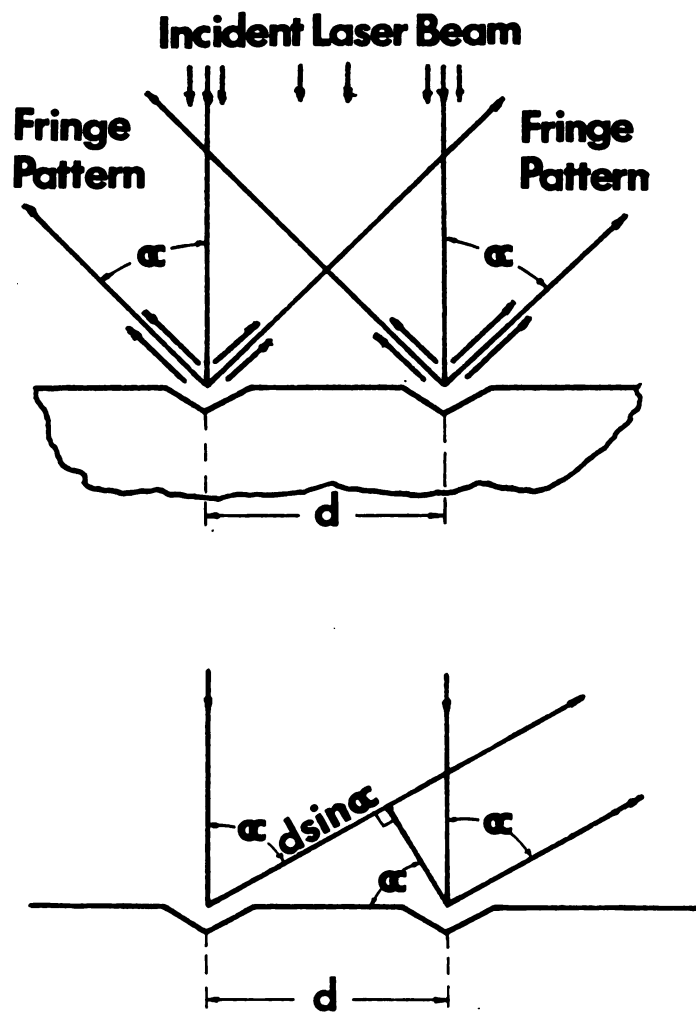


Figure 8 : Fringe Generation Principles



**Figure 9 : Indentations on Sample
(SEM Micrograph)**

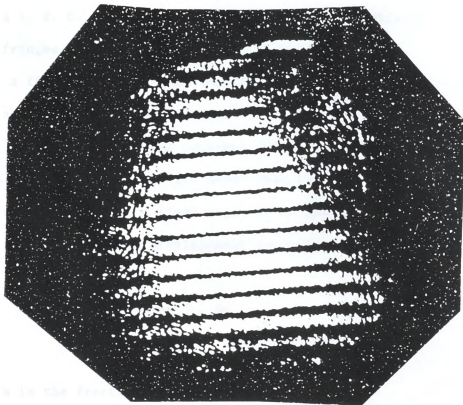


Figure 10 : Interference Pattern

α = angle between incident and reflected laser rays.

The interference fringes consist of consecutive bright and dark bands. Each bright fringe is defined by an integer, n , from equation (1). The I. S. G. measures strain by monitoring the movement of interference fringes.

For a fixed angle α_0 , when tensile load is applied to the specimen, the indentations move apart a distance δd . From equation (9) $d \sin \alpha_0 = n\lambda$, since λ is a constant for a given fringe, α_0 must decrease for tensile load, which means that the fringes will move toward the laser beam by δm , if a fixed angle α_0 is chosen. The relationship between fringe motion and displacement is defined as:

$$\delta d = \left(\frac{\lambda}{\sin \alpha_0} \right) \delta m \quad (10)$$

where, δm is the fraction of fringes.

A schematic diagram of the I. S. G. is shown in Figure 11. It has two channels. Fringe motion of both channels can also be caused by a rigid body motion which occurs in most loading. However, these effects are cancelled out since one pattern moves toward the laser while the other pattern moves away from it. Hence the relative displacement on the specimen can be averaged out by the following equation:

$$\delta d = \frac{\lambda}{\sin \alpha_0} \left(\frac{\delta m_1 + \delta m_2}{2} \right) \quad (11)$$

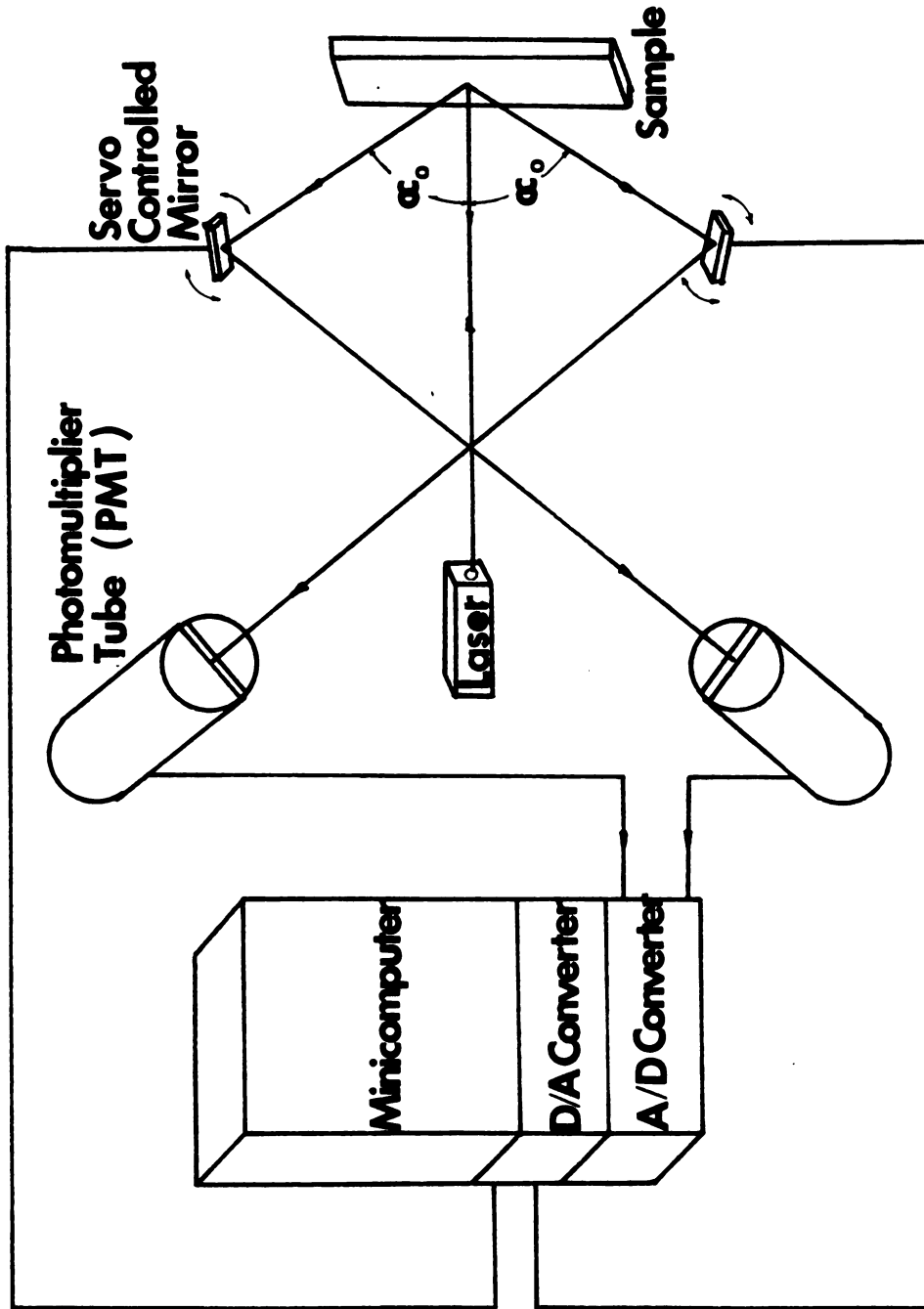


Figure 11: Schematic Diagram for the Laser Interferometric Strain Measuring System

The equation of strain can be expressed by:

$$\epsilon = \frac{\delta d}{d} = \frac{\lambda}{\sin \alpha_0} \left(\frac{\delta m_1 + \delta m_2}{2} \right) \quad (12)$$

Two servo mirrors located at two stationary observation points reflect the interference pattern onto slotted plates covering photomultiplier tubes (PMT's). The mirror position is controlled by a mini-computer which divides each sweep of the fringes into 256 consecutively numbered positions and stores the accompanying PMT voltage for each position. These data are converted to the analog strain (voltage) by using equation (12). A more detailed discussion of the I.S.G. may be found in Reference (14).

(f) Application of the I.S.G. Technique for an Epoxy Composite:

The interference pattern is formed by reflecting the laser beam from a very smooth surface. Unlike metallic materials, the polymeric composite materials are non-reflecting. Thus it was decided to metallize the surface by vapor deposition. Al, Au and Cu vapors were tried as the coating materials. Of these, Cu produces the best reflecting coating. However, after making indentations to obtain the interference patterns, there were several problems:

- (1) The interference patterns were very abnormal.
- (2) The reflecting angle was too small to make the fringe patterns appear on the servo mirrors.
- (3) Sometimes the indentations failed to produce fringe patterns.

After much trial and error and after microscopic inspection, it was concluded that problem (3) is due to the special property of glass-fibers. Because the glass-fiber deforms almost elastically as the indentations are applied to the sample, they bounce back after the indentation load is removed (Figure 12). The net effect causes the surface of indentation to be irregular which in turn destroys a regular and periodic fringe pattern.

In order to avoid this problem, we tried to make indentations in the regions that contain only epoxy. These results show that although it is possible to get fringe patterns, problems (1) and (2) still exist. From Figure 13, it is obvious that, because of the viscoelastic recovery of epoxy, the surface of the indentation bounces back with time. This would decrease the angle α to α' (where α' is a function of time). This is the reason why the angle of the indented surface is too small to produce a fringe pattern on the servo mirror. Also at various portions of an indentation there are different degrees of relaxation. Thus a slightly curved and rough vapor deposited surfaces are produced. An attempt to make a stable indentation shape by allowing creep flow (i.e. to leave the major indentation load longer) also failed to solve this problem.

Knowing these reasons, we believed that the only way to solve these problems was to avoid the indentation into the composite material. The next step was, then, to increase the thickness of the deposition layer. From Figure 14, the thickness of the layer should

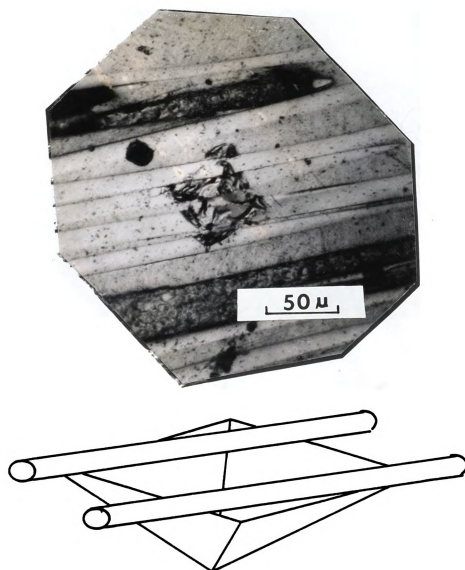


**Figure 12 : The Indentation in the Region
That Contains Both Fibers and
Epoxy**

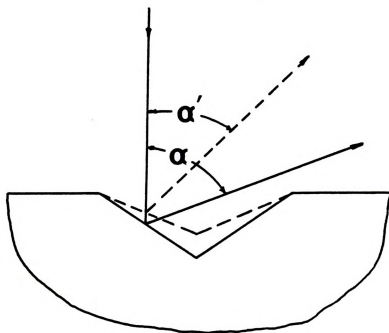
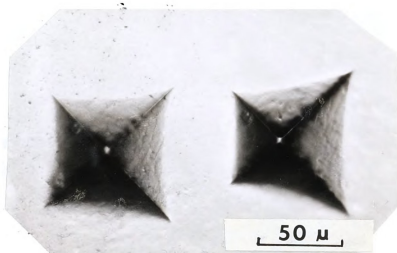


**Figure 13 : Indentations in the Region That
Contains Epoxy Only**

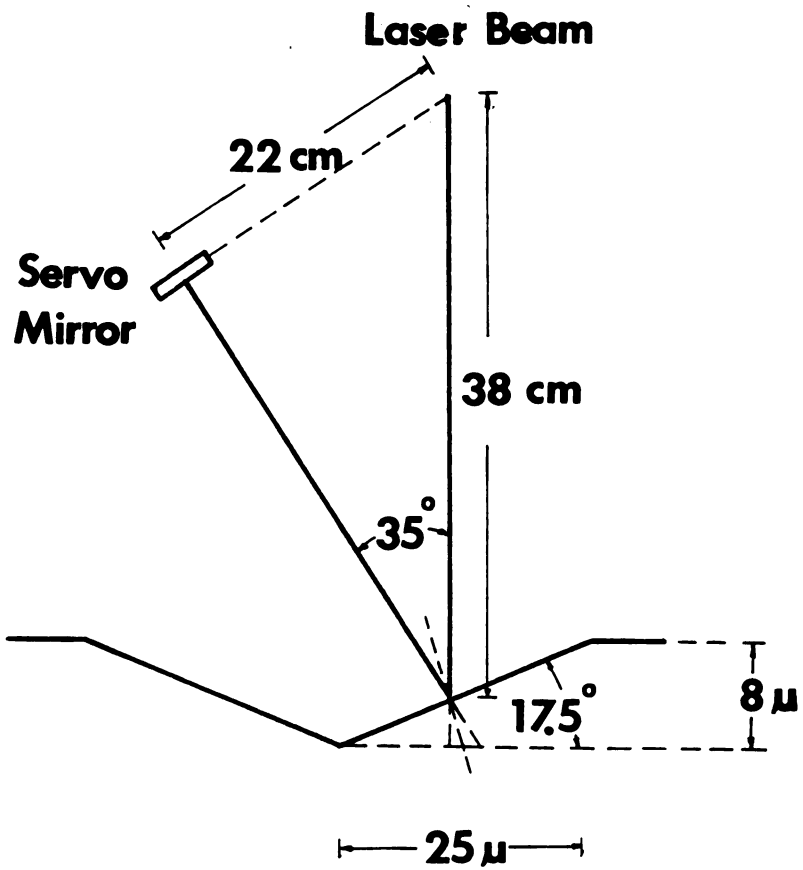


Figure 14 : Geometry of the Indentation

be over 8 microns. Unfortunately as the thickness of the deposition increases, the surface of the deposition becomes rough and less reflecting. We thus have to polish the surface after vapor deposition. But the bonding between the deposited layer and the sample is not very strong and hence the layer tends to peel off during metallographic polishing.

Several attempts were made to circumvent these problems. The final solution was to bond an aluminum foil on the sample. Using "M-Bond", an aluminum foil can be bonded to the sample. Since the surface of the aluminum foil is not very smooth, it was necessary to polish the sample surface by metallographic techniques after bonding the aluminum foil. Microhardness indentations were then successfully and easily produced on the metallized surface (Figure 9). Interference fringe patterns from such surfaces are well formed and quite reproducible. A clip-on extensometer was used to check the validity of the I.S.G. technique for this composite material.

(g) Cyclic Stress-Strain Test:

A computer controlled closed-loop MTS testing machine was used to perform all of the cyclic tests. Woods metal grip was used for the sample grip so that sample could be mounted in a stress free condition.

Before testing, the aluminum foil was bonded on the sample. After polishing the foil surface indentations were applied. One set of indentations were across the width of the sample in order to determine the distribution of σ_x across the top layer. For the calibration



test, strain was measured with the I.S.G. as well as by using a MTS extensometer (model #632, 13B 20).

III. EXPERIMENTAL RESULTS AND DISCUSSION

(a) Static Tensile Properties:

The fibers are the principal reinforcing or load-carrying agents. They are typically strong and stiff and generally exhibit a linear elastic behavior (Figure 15). The function of the epoxy matrix is to support and protect the fibers, and to provide a means of distributing the load among the fibers. The epoxy itself, generally exhibits a viscoelastic behavior (Figure 16). Because the fibers provide the majority of the strength and stiffness, the fiber-reinforced composite is treated as a linear elastic material. The results of the stress-strain curves (Figure 17) elucidate this phenomenon.

The experimental stress-strain curves of 0° directional sample can be easily separated into three regions (Figure 18).

Region I: (the linear portion at lower stresses)

In this region, both the glass-fiber and the epoxy are within the elastic limits.

Region II: (the curved region)

In this region, the stress has already reached the yield strength of the epoxy, i.e. the fiber continues to deform elastically, but the epoxy deforms plastically.

Region III: (the linear portion at higher stresses)

In this region, because of the high stress, the

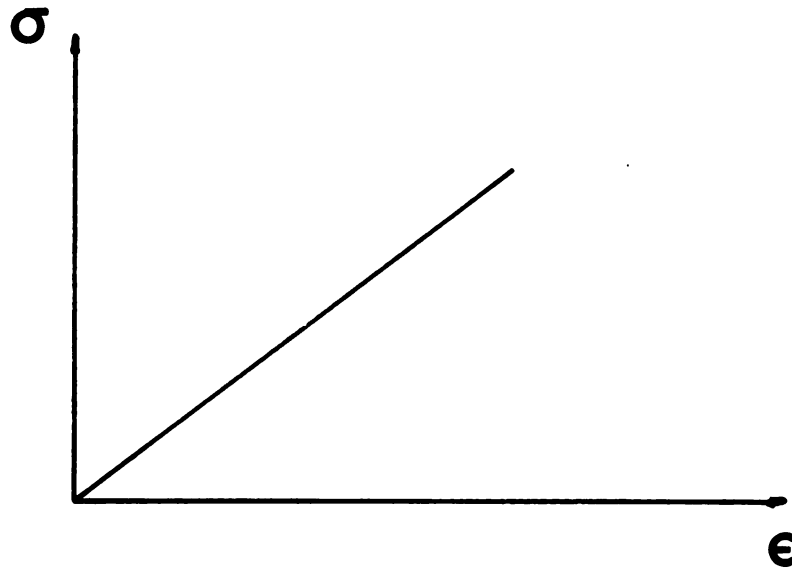


Figure 15 : Schematic Stress-Strain Behavior of a Linear Elastic Material

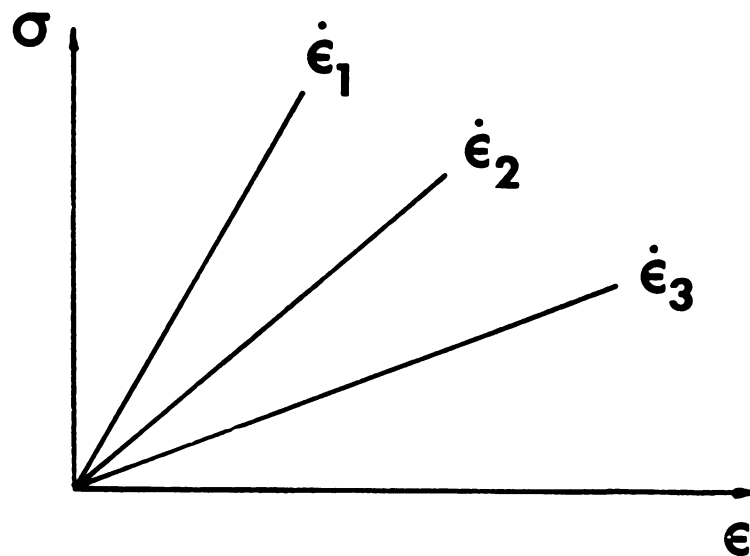


Figure 16 : Schematic Stress-Strain Behavior of a Viscoelastic Material ($\dot{\epsilon}_1 > \dot{\epsilon}_2 > \dot{\epsilon}_3$)

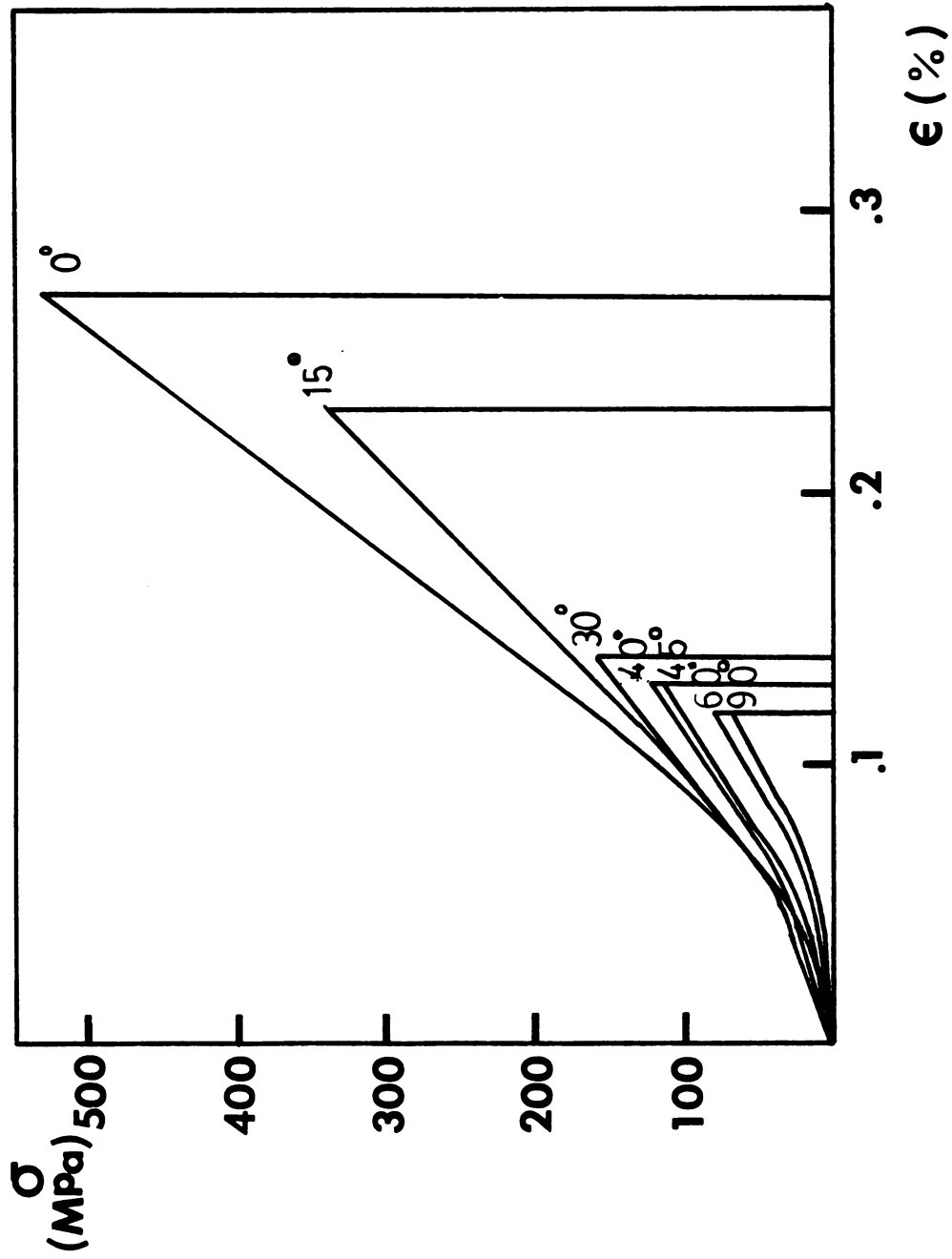


Figure 17 : Tensile Stress - Strain Curve of the Composite for Different Orientations

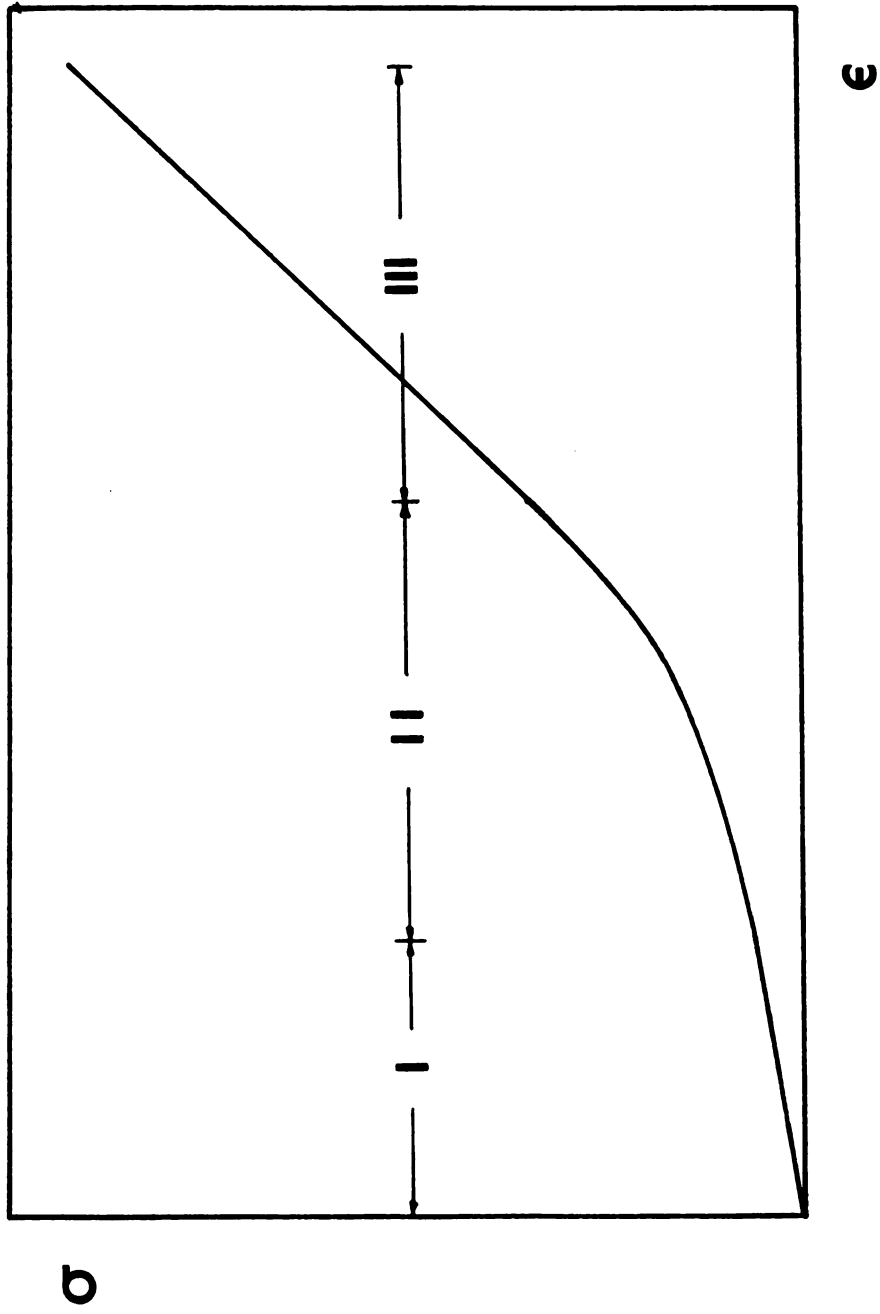


Figure 18: Schematic Presentation of the Three Regions of the Tensile Stress - Strain Curve

epoxy is no more able to carry the load and the stress is carried by the glass-fibers only. This region is again linear and reflects the linear elastic behavior of glass-fibers.

(b) Failure Criterion:

Figure 19 has shown that there are essentially two different failure modes in these samples. For smaller angles of θ (approximately $0^\circ - 10^\circ$), the fracture surface is "brush-like" and a severe delamination occurs which extends inside the grip section of the sample. For larger angles, θ greater than 10° , the fracture surface is clean and very little delamination occurs.

These two modes can be explained by the scanning electron microscopic pictures of the fracture surface. Under the tension test, the strain is the same for the glass-fiber and the epoxy. However, the glass-fiber has a higher elastic modulus from that of the epoxy, therefore, the stress of the fiber would be larger than that of epoxy. Thus a matrix shear stress would result at the interface. For the 0° samples, all the load is carried by the fibers. The matrix shear stress could not exceed the strength of the fiber, but could exceed the allowable matrix shear stress. Therefore, delamination would occur before the fibers are broken (Figure 20). After the stress reaches the fracture strength some of the fibers would be broken, followed by cumulative fiber failure across the sample, and hence cause the overall fracture of the composite. Therefore, the fracture surface would

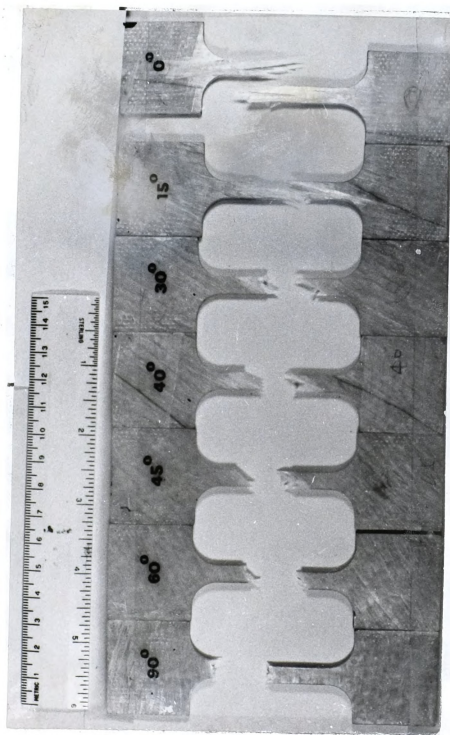
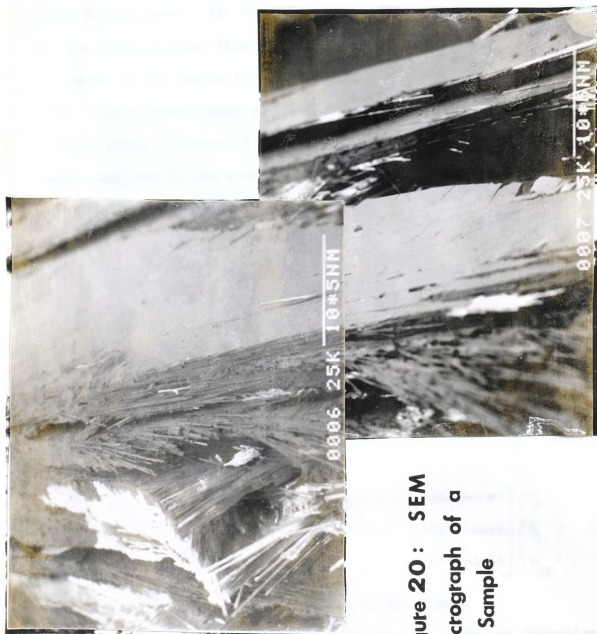


Figure 19: Comparison of Fracture Surface for Various Orientations



**Figure 20 : SEM
Micrograph of a
0° Sample**

appear brush-like and delaminated surface. This failure mode is called fiber-failure mode. For the 90° samples, the load is not all carried by the unidirectional fibers, the only fibers which can carry the load are those in the random layers and lie parallel to the loading direction. Since those fibers are relatively few in number, the sample will be broken by means of debonding between the fiber and the epoxy matrix followed by the propagation of this crack perpendicular to the tensile axis (Figure 21, 22). Therefore, the fracture surface would be very clean. This failure mode is called matrix-failure mode.

Consider the lamina as shown in Figure 23. There, the coordinates of the applied stress axes are X and Y; whereas the principal coordinates (with respect to the unidirectional fiber orientation) are 1 and 2. The transformation equations for expressing stresses in an 1-2 coordinate system in terms of stresses in an X-Y coordinate system (See appendix A) are

$$\begin{Bmatrix} \sigma_1 \\ \sigma_2 \\ \sigma_{12} \end{Bmatrix} = \begin{bmatrix} \cos^2\theta & \sin^2\theta & 2\sin\theta\cos\theta \\ \sin^2\theta & \cos^2\theta & -2\sin\theta\cos\theta \\ -\sin\theta\cos\theta & \sin\theta\cos\theta & \cos^2\theta - \sin^2\theta \end{bmatrix} \begin{Bmatrix} \sigma_x \\ \sigma_y \\ \sigma_{xy} \end{Bmatrix} \quad (13)$$

where θ is the angle from the X-axis to the 1-axis.

Since a uniform uniaxial stress σ was applied in the direction of X-axis, the state of stress is then

$$\begin{aligned} \sigma_x &= \sigma \\ \sigma_y &= \tau_{xy} = 0 \end{aligned} \quad (14)$$



Figure 21 : SEM Micrograph of a 90° Sample



**Figure 22: SEM Micrograph of a 90° Sample
(750 x)**

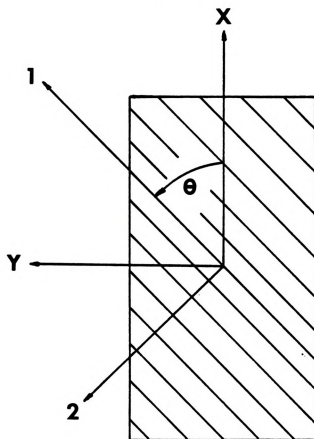


Figure 23: Positive Rotation of Principal Material Axes from Arbitrary X-Y Axes

Hence equation (13) can be simplified as

$$\begin{aligned}\sigma_1 &= \sigma \cos^2 \theta \\ \sigma_2 &= \sigma \sin^2 \theta \\ \tau_{12} &= \sigma \sin \theta \cos \theta\end{aligned}\tag{15}$$

Since these two failure modes have different failure mechanisms, it may be assumed that they are independent. For the fiber-failure mode, we shall assume that the fracture strength σ_f equates to $\sigma_0 \cos^2 \theta$, where σ_0 is the fracture strength of 0 degree orientation because for small angles, the factor of $\cos^2 \theta$ will not change very much. For the matrix-failure mode, we shall assume that it is a function of σ_2 and τ_{12} . Thus, for fiber failure mode and matrix failure modes respectively, we have:

$$\sigma_f = \sigma_0 \cos^2 \theta \tag{16.a}$$

$$F(\sigma_2, \tau_{12}) = 1 \tag{16.b}$$

It has been proposed (2) that $F(\sigma_2, \tau_{12}) = 1$ can be written in the form:

$$\left(\frac{\sigma_2}{\sigma_2^s}\right)^n + \left(\frac{\tau_{12}}{\tau_{12}^s}\right)^n = 1 \tag{17}$$

where σ_2^s and τ_{12}^s are material constants.

Substituting equation (15) into equation (17), it follows that

$$\sigma_f = \sigma_o \cos^2 \theta$$

$$\left(\frac{\sigma_o}{\sigma_s} \right)^n \sin^{2n} \theta + \left(\frac{\sigma_m}{\tau_{12}} \right)^n \sin^n \theta \cos^n \theta = 1 \quad (18)$$

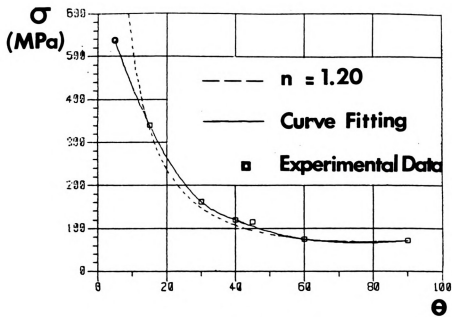
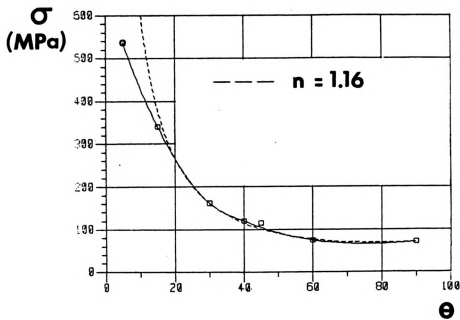
where σ_f is the fracture strength in the fiber failure region and σ_m is the fracture strength in the matrix failure region. By the Newton interpolation polynomial method and equation (17), it is found that n is equal to 1.16 (Figures 24, 25). At the critical angle θ_c , which is the transition point, both failure criteria should hold at the same time; namely, $\sigma_f = \sigma_m = \sigma_c$. Then,

$$\sigma_c = \sigma_o \cos^2 \theta_c$$

$$\left(\frac{\sigma_c}{\sigma_s} \right)^n \sin^{2n} \theta_c + \left(\frac{\sigma_c}{\tau_{12}} \right)^n \sin^n \theta_c \cos^n \theta_c = 1 \quad (19)$$

Eliminating σ_c from equation (19),

$$\left(\frac{\sigma_o}{\sigma_s} \right)^n \sin^{2n} \theta_c \cos^{2n} \theta_c + \left(\frac{\sigma_o}{\tau_{12}} \right)^n \sin^n \theta_c \cos^{3n} \theta_c = 1 \quad (20)$$

Figure 24: $n = 1.20$ Figure 25: $n = 1.16$

Since

$$n = 1.16$$

$$\sigma_o = 537 \text{ Mpa}$$

$$\sigma_2^s = 71 \text{ Mpa}$$

$$\tau_{12}^s = 119.6 \text{ Mpa}$$

θ can be calculated by using a computer. The value of θ_c determined this way is:

$$\theta_c = 10.7^\circ$$

This angle shows a very good agreement with the experimentally observed value (Figure 19). Both curves of different failure criteria are plotted in Figure 26. and a good correspondence between the experimental points and the calculated curves are seen.

(c) Validity of I.S.G. Technique for Composites:

From the extensometer, the Young's Modulus of the sample is determined to be 37040 Mpa (Figure 27) and the average value of the modulus obtained by using the I.S.G. is 37550 Mpa. Since the composite materials are a heterogeneous and elastically nonlinear material, the Young's Modulus will have a different value as the location of the micro-gauge section changes. Hence the difference of 1.76% between the average value of modulus from the I.S.G. and that from the clip-on gauge is within the reasonable limit. Thus the strain in aluminum

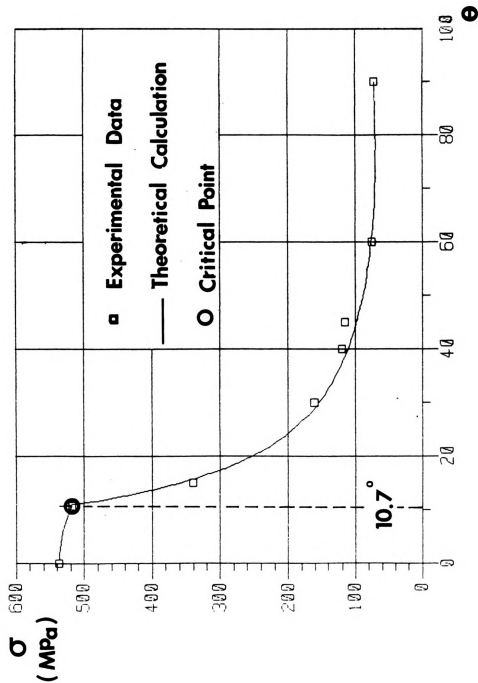


Figure 2 6: Static Strength vs. Angle

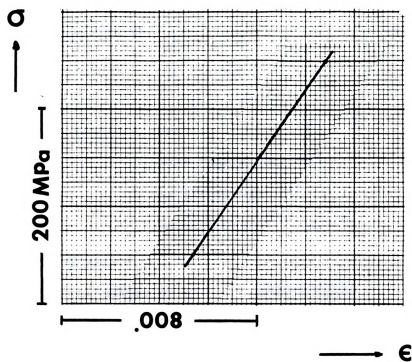


Figure 27: Extensometer Strain vs. Stress

foil is the same as that in the composite materials (no aluminum foil was used while the clip-on gauge was employed). The thickness of the aluminum foil used in these experiments is very small (≈ 10 microns) and thus the reinforcement effect can be neglected. Since the aluminum foil does not extend to the grip sections, the load is not directly transmitted via the aluminum foil. Hence the response of the aluminum foil by the grip will also be neglected.

(d) Stress Distribution Across the Top Surface:

Theoretical predictions of Pagano (8), Wang and Crossman (9) state that surface stress along the tensile axis decreases as the parameter Y/b increases, where b is the half width of the sample, Y is the distance along the Y axis from the central vertical plane of the sample. Figure 28 shows the nature of this decrease as predicted by Pagano (8), Wang and Crossman (9). Although we do not have sufficient number of experimental points, it is interesting to note that the σ_x value near the edge of the sample is lower than that near the central stress axis. Two experimental data points (full circles) are shown in Figure 28. Considering the experimental uncertainties and the limited data, the agreement between the theoretical curve of Wang and Crossman, and the two experimental points seems to be interesting. Detailed and systematic experiments, however, are needed to confirm this observation.

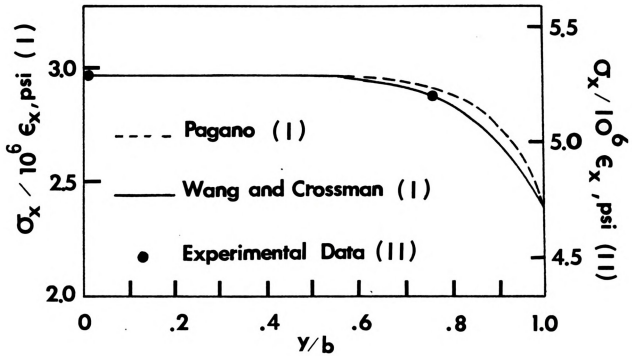


Figure 28 : Distribution of σ_x along Surface of the Sample for a Constant Strain 10^{-6}

IV. CONCLUSIONS

Based on the information obtained, the following conclusions can be reached:

1. For this special material, the failure criterion can be expressed by two simple equations. For fiber failure mode and matrix failure mode respectively, we have:

$$\sigma_f = \sigma_o \cos^2 \theta$$
$$\left(\frac{\sigma_m}{\sigma_s} \right)^n \sin^{2n} \theta + \left(\frac{\tau_m}{\tau_s} \right)^n \sin^n \theta \cos^n \theta = 1$$

where n is 1.16 for this material.

2. The I.S.G. can be successfully applied to the composite materials. This is a very powerful technique which can determine the stress distribution by measuring the local stress-strain behaviors.
3. The free edge effect has been shown by experimental results.
4. The stress distribution that was measured by the I.S.G. has been compared well with the theoretical prediction of Wang and Crossman (9), and Pagano (8).

APPENDIX

The transformation of stresses state from X,Y and Z coordinates to 1,2 and 3 coordinates can be expressed as following:

$$\begin{bmatrix} \sigma_{11} & \sigma_{12} & \sigma_{13} \\ \sigma_{21} & \sigma_{22} & \sigma_{23} \\ \sigma_{31} & \sigma_{32} & \sigma_{33} \end{bmatrix} = \begin{bmatrix} & & \\ & A & \\ & & \end{bmatrix} \begin{bmatrix} \sigma_{xx} & \sigma_{xy} & \sigma_{xz} \\ \sigma_{yx} & \sigma_{yy} & \sigma_{yz} \\ \sigma_{zx} & \sigma_{zy} & \sigma_{zz} \end{bmatrix} \begin{bmatrix} & & \\ & A & \\ & & \end{bmatrix}^T$$

From Figure 23, it is an in-plane stresses state and rotated an angle about Z-axis. Therefore, the relationship (a) can be simplified as:

$$\begin{bmatrix} \sigma_{11} & \sigma_{12} & 0 \\ \sigma_{21} & \sigma_{22} & 0 \\ 0 & 0 & 0 \end{bmatrix} = \begin{bmatrix} \cos\theta & \sin\theta & 0 \\ -\sin\theta & \cos\theta & 0 \\ 0 & 0 & 1 \end{bmatrix} \begin{bmatrix} \sigma_{xx} & \sigma_{xy} & 0 \\ \sigma_{yx} & \sigma_{yy} & 0 \\ 0 & 0 & 0 \end{bmatrix} \begin{bmatrix} \cos\theta & -\sin\theta & 0 \\ \sin\theta & \cos\theta & 0 \\ 0 & 0 & 1 \end{bmatrix}$$

$$\begin{bmatrix} \sigma_{11} & \sigma_{12} & 0 \\ \sigma_{21} & \sigma_{22} & 0 \\ 0 & 0 & 0 \end{bmatrix} = \begin{bmatrix} \sigma_{xx}\cos^2\theta + 2\sigma_{xy}\sin\theta\cos\theta + \sigma_{yy}\sin^2\theta \\ -\sigma_{xx}\sin\theta\cos\theta + \sigma_{xy}(\cos^2\theta - \sin^2\theta) + \sigma_{yy}\sin\theta\cos\theta \\ 0 \\ -\sigma_{xx}\cos\theta\sin\theta + \sigma_{xy}(\cos^2\theta - \sin^2\theta) + \sigma_{yy}\sin\theta\cos\theta \\ \sigma_{xx}\sin^2\theta - 2\sigma_{xy}\sin\theta\cos\theta + \sigma_{yy}\cos^2\theta \\ 0 \end{bmatrix}$$

Hence,

$$\begin{Bmatrix} \sigma_{11} \\ \sigma_{22} \\ \sigma_{12} \end{Bmatrix} = \begin{bmatrix} \cos^2 \theta & \sin^2 \theta & 2\sin \theta \cos \theta \\ \sin^2 \theta & \cos^2 \theta & -2\sin \theta \cos \theta \\ -\sin \theta \cos \theta & \sin \theta \cos \theta & \cos^2 \theta - \sin^2 \theta \end{bmatrix} \begin{Bmatrix} \sigma_{xx} \\ \sigma_{yy} \\ \sigma_{xy} \end{Bmatrix}$$

REFERENCES

1. Tsai, S. W. and Wu, E. M., "A General Theory of Strength for Anisotropic Materials." Journal of Composite Material, Vol. 5 (1971), p. 58.
2. Hashin, Z. and Rotem, A., "A Fatigue Failure Criterion for Fiber Reinforced Materials," Journal of Composite Materials, Vol. 7 (1973), p. 448.
3. Rotem, A. and Hashin, Z., " Fatigue of Angle Ply Laminates," AIAAJournal, Vol. 14 (1970), p.271.
4. Rotem, A., "Fatigue Failure of Multidirectional Laminate," AIAA Journal, Vol. 17 (1979), p. 271.
5. Puppo, A. H. and Evenson, H. A., " Interlaminar Shear in Laminated Composites Under Generalized Plane Stress," Journal of Composite Materials, Vol. 4 (1970), p. 204.
6. Pipes, R. B. and Pagano, N. J., "The Influence of Stacking Sequence on Laminate Strength," Journal of Composite Materials, Vol. 5 (1971) , p. 50.
7. Pipes, R. B., "Moiré Analysis of the Interlaminar Shear Edge Effect in Laminated Composites," Journal of Composite Materials, Vol. 5 (1971), p. 255
8. Pagano, N. J., "Stress Fields in Composite Laminates," International Journal of Solid Structure, Vol. 14 (1978), p. 385.
9. Wang, A. S. D. and Crossman, F.W., "Some New results on Edge Effect in Symmetric Composite Laminates," Journal of Composite Materials, Vol. 11 (1979), p. 92
10. Pipes, R. B., and Pagano, N. J., "Interlaminar Stress in Composite Laminates Under Axial Extension," Journal of Composite Material, Vol. 4 (1970), p. 538.
11. Wang, S. S. and Wang, H. T., "Interlaminar Crack Growth in Fiber Reinforced Composites During Fatigue," Journal of Engineering Materials and Technology, Vol. 101 (1979), p. 34.
12. Sharpe, W. N. Jr., "The Interferometric Strain Gage," Experimental Mechanics, Vol. 8, No. 4 (1968), p. 164.

13. Sharpe, W. N. Jr., "A Short Gage Length Optical Gage for Small Strain," *Experimental Mechanics*, Vol. 14, No. 9 (1974), p. 373.
14. Bofferding, C. H. "A Study of Cycle Stress and Strain Concentration Factor at Notch Roots Throughout Factors Life," Master Thesis, Michigan State University, 1980.
15. Lucas, L. J., "Experimental Verification of the Neuber Relation at Room and Elevated Temperature," Master Thesis, Michigan State University, 1982.

MICHIGAN STATE UNIVERSITY LIBRARIES



3 1293 03046 2299